

Unfolding axial caustics of glory scattering with harmonic angular perturbations of toroidal wave fronts^{a)}

W. Patrick Arnott^{b)} and Philip L. Marston

Department of Physics, Washington State University, Pullman, Washington 99164-2814

(Received 8 August 1988; accepted for publication 28 November 1988)

Axisymmetric toroidal wave fronts are pertinent to the near forward and backward scattering by objects that have rotational symmetry. For spheres, the wave field produced by such a wave front is known as glory scattering. As the wave front propagates, some portion of it becomes focused on an axis, forming a structurally unstable line caustic. A specific class of harmonic perturbations of the wave front shape is considered that leads to unfoldings of the axial caustic. When the wave front shape is perturbed to have two-fold rotational and mirror symmetry, the unfolded caustic is a four-cusped astroid curve. The three-fold symmetric perturbed wave front propagates to produce a hypocycloid caustic with three cusps. In general, perturbed wave fronts with p -fold rotational and mirror symmetry have caustics of cusped stars, with p cusps when p is odd, and $2p$ cusps when p is even. These wave front perturbations have applications to scattering from symmetric, slightly nonspherical, homogeneous objects such as spheroids. Wave fields are computed using a Fresnel approximation of the diffraction integral. The wave field patterns associated with astroid caustics are displayed. They have features similar to Pearcey patterns. Applications to backscattering from spheroids, distorted torii, and axicon reflectors are noted. Certain inverse problems are considered. An inequality is given for determining the magnitude of wave front perturbations needed to cause a significant change in the wave field from that of a spherical scatterer. The merging of rays as the observation direction moves across the caustic is discussed using concepts from catastrophe optics. A novel expression in polar coordinates is given for the Hessian associated with propagation.

PACS numbers: 43.20.Fn, 43.20.Bi, 43.30.Gv

INTRODUCTION

A wide range of spherical scatterers produce backward or forward directed toroidal wave fronts of the type shown in Fig. 1(a) (Refs. 1–12). These wave fronts give rise to glory scattering. The wave fields associated with this wave front have been discussed previously.^{1–12} The present work was motivated by the desire to *understand what happens to the caustic and to the scattered wave fields when the symmetry of the scatterer deviates slightly from the spherical shape*. Consider, e.g., a slightly oblate spherical scatterer made of the same materials considered in Refs. 1–11. This shape is generated by rotating an ellipse about its semiminor axis. The oblate spheroid has two-fold rotational and mirror symmetries and inversion symmetry about any axis which lies in the equatorial plane and is perpendicular to the axis of rotational symmetry (the semiminor axis). Consider a plane wave traveling perpendicular to the axis of rotational symmetry and incident upon the oblate object. The propagation direction is parallel to an axis of two-fold symmetry.¹³ The resulting backward or forward scattered wave fronts should have the same symmetry as the oblate spheroidal object has for sufficiently small deformations from the spherical shape. An important subclass of such wave fronts is a toroidal wave front having a superimposed harmonic angular perturbation described by Eq. (10) below and shown in Fig. 1(b).

To simplify the presentation, we take the expression p -fold symmetry to imply *both* p -fold rotational symmetry about the z axis in Fig. 2, and p -fold mirror symmetry about planes parallel to this axis. All of the scatterers, wave fronts, and caustic surfaces considered in this article have at least both of these symmetries (see Fig. 6, for example).

We have used the wave front shape in Fig. 1(b) to model the backscattering of horizontally propagating laser light by freely rising oblate spheroidal air bubbles in water.¹⁴ Model calculations of the angular scattering patterns agree favorably with observations. In the present article, we consider only scalar (acoustic) wave fields. The caustics described are for a wider range of scattering symmetries than those of Ref. 14.

In Sec. I, we briefly review the theory of caustic formation in general scattering problems. The propagation properties of the axisymmetric wave front in Fig. 1(a) are briefly discussed, and the explicit form of the harmonically perturbed toroidal wave front shown in Fig. 1(b) is given. Other surfaces that should give wave fronts like that of Fig. 1(b) are discussed. These results are generalized to wave fronts and certain scatterers with p -fold rotational and mirror symmetries in Sec. I D. The caustic surface associated with the general harmonically perturbed wave front is computed in Sec. I E. Application to axicons^{15–19} are noted in Appendix B.

In Sec. II A, the wave field associated with the general harmonically perturbed wave front is computed using the Rayleigh–Sommerfeld diffraction theory²⁰ in the Fresnel approximation. Computational results for the wave field and

^{a)} Portions of this work were presented at the 115th Meeting of the Acoustical Society of America [J. Acoust. Soc. Am. Suppl. 1 **83**, S59 (1988)].

^{b)} Present address: National Center for Physical Acoustics, P. O. Box 847, University, MS 38677.

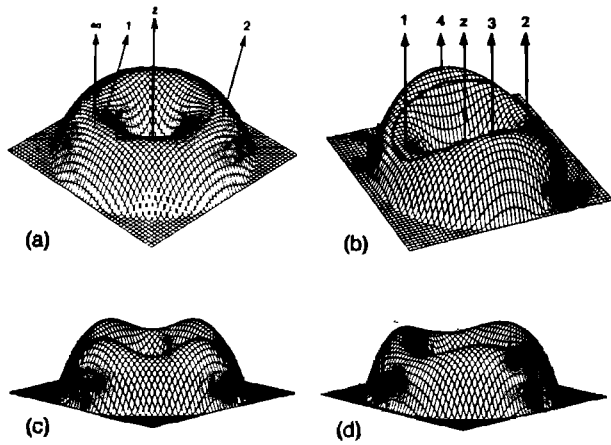


FIG. 1. (a) The axisymmetric toroidal wave front of Eq. (9), near the exit plane of Fig. (2), which propagates to form an axial caustic. The ring on top is the zero Gaussian-curvature contour (ZGCC) of the wave front. An infinite number of rays (like the ray labeled ∞), emanate from the ZGCC and are focused in the direction of the z axis. (b) The harmonically perturbed wave front of Eq. (10) and Eq. (15) with $p = 2$. The ZGCC is sketched on this wave front as the dark distorted ring. In contrast to (a), only the (now unfocused) four rays labeled 1-4 are backward directed. (c) and (d) are harmonically perturbed wave fronts for $p = 4$ and 3 in Eq. (15).

caustics are given in Sec. II B. An expression is given in Sec. II C for the minimal wave front perturbation necessary to observe effects of the harmonic perturbation in the angular scattering pattern for a given wavelength. Combined use of the wave field and caustic calculations allows derivation of expressions useful for inverse scattering.

In Sec. III, some detailed properties of the rays introduced in Sec. I are discussed for rays associated with the wave front in Fig. 1(b). These properties should be useful for predicting the time delays occurring for the scattering of pulsed sound by oblate objects and are necessary for a more thorough understanding of the scattering process. In Sec. IV, the connection between this work and catastrophe theory, as it applies to wave propagation problems,^{21,22} are developed. In particular, we find that certain local regions of the wave front shown in Fig. 1(b) are special cases of the more general class of wave front studied by Marston²³ that give transverse cusp diffraction catastrophes on propagation.²⁴ (Readers primarily interested in Secs. I E and II may skip the applications introduced in Secs. I B and C and Appendix B.)

Though the emphasis of the present article is on propa-

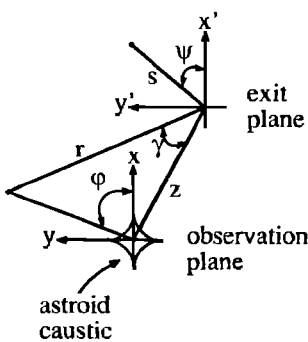


FIG. 2. Coordinate system for the caustic and wave field calculations. The initial wave front is specified near the exit plane and propagates towards the observation plane. For sufficiently large z , the caustic shape in the observation plane for the wave front shown in Fig. 1(b) is an astroid curve. Polar coordinates (s, ψ) specify points in the exit plane while the observation point is specified by (γ, ϕ, z) .

gation in homogeneous media, it may be argued that unfoldings considered are germane to perturbations in the scattering from spheres caused by certain stratified media.

The method of physical optics presented here gives geometrical insight into the scattered wave fields. This method is applicable to a restrictive group of scatterers, namely objects that give wave fronts with geometries that satisfy the inequality in (21). A requirement of this method is that the objects have sufficiently large size parameters [roughly, $kb \geq 15$, where k is the wavenumber of the incident radiation and b is a characteristic dimension discussed below Eq. (9)]. Partial-wave series and T -matrix solutions for the boundary value problems can produce accurate and general descriptions of scattered wave fields; however, these solutions, in themselves, do not always give the desired physical insight. For large size parameters, such solutions can become numerically unstable, and physical optics solutions become more useful if not necessary. In the limit that the size parameter goes to infinity, the size of diffracton fringes goes to zero, and the mathematical focusing of wave fronts to form caustics as discussed in Sec. I becomes the only necessary piece of information. In this limit, the wave field has a divergent amplitude on caustics. It often turns out that the physical optics model appropriate for one type of scatterer is useful for gaining insight into other scatterers. This point is amply illustrated in the present work.

I. RAYS AND CAUSTICS OF HARMONICALLY PERTURBED TOROIDAL WAVE FRONTS

A. Caustic surfaces associated with general wave fronts

The relevant coordinate system is shown in Fig. 2. The initial wave front W is specified near an exit plane having Cartesian coordinates x' and y' . Polar coordinates s (radial distance) and ψ (azimuthal angle) are also used to address points in the exit plane. The instantaneous displacement of the wave from the exit plane is given by $W(x', y')$ (Refs. 21 and 22). For example, W could be the wave front shape resulting when an initially spherical wave passes through a medium with inhomogeneities localized between a source and the exit plane. We are concerned with waves that propagate from near the exit plane to an observation plane parallel to the exit plane, and displaced by a distance z . Cartesian coordinates (x, y, z) define points in the observation plane. Observation plane points are also given by the backscattering angle γ , the distance r , and the azimuthal angle ϕ .

Strictly geometrical considerations give much useful information about the focal properties of W (Refs. 21 and 22). Consider the surface $z = W(x', y')$. Each point on W has, in general, two principle radii of curvature, R_j with $j = 1, 2$. [The Gaussian curvature is $K = (R_1 R_2)^{-1}$.] The vector $S = [x', y', W(x', y')]$ locates points on W . Let the vector N be the unit normal of W . Then, from the vectors $P = NR_j + S$. Denote the z component of P as P_z . The surface formed by the locus of all P with $P_z(x', y') > W(x', y')$ is the caustic surface associated with W . We may, likewise, define a source (real or virtual) as the locus of all P with $P_z < W$. These are the focal surfaces of W . In the present

investigation, we are interested in the regions of W for which the assumption that \mathbf{N} is nearly parallel to the z axis is a good approximation. This paraxial assumption greatly simplifies the analysis. Direct calculation of \mathbf{P} is a point by point process; another approach is analytically more tractable.

We may define a distance function

$$\phi = \{(x - x')^2 + (y - y')^2 + [z - W(x', y')]^2\}^{1/2} \quad (1)$$

as the distance from a point on W to the observation point (x, y, z) . Rays are line segments from $(x', y', W(x', y'))$ to (x, y, z) for which the condition

$$\phi_{x'} = 0, \quad \phi_{y'} = 0 \quad (2)$$

applies. Here, the subscript x' refers to partial differentiation with respect to the x' variable, etc. These line segments are orthogonal to W and are the familiar rays of geometrical optics. Equation (2) is equivalent to Fermat's principle for homogeneous media. The condition expressed by (2) defines a mapping of points from the exit plane to the observation plane.

In the geometrical optics, energy flux travels along the rays.^{21,22} Denote the energy flux (i.e., the power per unit area) for a local region of W as $I'(x', y')$ and, similarly, $I(x, y)$ for the energy flux in the observation plane. Denote ν as the angle between the z axis and the ray propagation direction. By power conservation, we expect the energy flux associated with a bundle of rays passing through area $dx' dy' / \cos \nu$ to remain constant as the rays propagate to the observation plane, where the ray bundle has cross-sectional area $dx dy \cos \nu$. (The $\cos \nu$ factors are necessary to give the ray bundle area normal to the propagation direction.) The expression for power conservation in geometrical optics is $I'(x', y') dx' dy' = I(x, y) dx dy \cos^2 \nu$. Using $dx dy = |J(x', y')| dx' dy'$, the energy flux propagated to the observation plane via (2) is $I(x, y) = I'(x', y') / |\cos^2 \nu J(x', y')|$, where J is the Jacobian of the transformation defined by (2). It may be shown that $J = \phi^2 H$, where H is the Hessian^{21,22}:

$$H = \phi_{x'x'} \phi_{y'y'} - \phi_{x'y'}^2 \quad (3)$$

Thus geometrical optics predicts $I(x, y)$ to be infinite on the surface defined by Eq. (2), with $H(x', y'; x, y, z) = 0$. The area associated with a bundle of rays has shrunk to zero on this surface. This surface is known as the caustic surface. Diffraction effects on and near the caustic surface soften this infinity. Catastrophe theory^{21,22} can be used to classify many of the singularities (i.e., $H = 0$) of the gradient map [the ray equation (2)].

Equations (1)–(3) may be simplified by use of a paraxial assumption, which consists of the following: $W/z, W_x^2, W_y^2$, and $W_x W_y$ are all $\ll 1$. The distance function becomes

$$\begin{aligned} \phi(x', y'; x, y, z) = & z - W(x', y') \\ & + \frac{x^2 + y^2}{2z} + \frac{x^2 + y^2}{2z} - \frac{xx' + yy'}{z} \end{aligned} \quad (4)$$

Using the polar coordinate system of Fig. 2, (4) becomes

$$\phi(s, \psi; \gamma, \varphi, z) = r - W(s, \psi) + s^2/2z - s \sin \gamma \cos(\psi - \varphi) \quad (5)$$

The approximations $r \approx z + (x^2 + y^2)/2z$, and $\tan \gamma \approx \sin \gamma$

were used in going from (4)–(5). The ray condition given by (2) can be written as

$$\begin{pmatrix} x \\ y \\ z' \\ z \end{pmatrix} \equiv (U, V) = \begin{pmatrix} \cos \psi Q_s - \frac{\sin \psi}{s} Q_\psi, \\ \sin \psi Q_s + \frac{\cos \psi}{s} Q_\psi \end{pmatrix}, \quad (6)$$

where subscripts denote differentiation and Q is given by

$$Q(s, \psi; z) = s^2/2z - W(s, \psi) \quad (7)$$

Using the approximate form for the distance function (5), the Hessian in (3) becomes

$$H(s, \psi; z) = \frac{Q_s Q_{ss}}{s} + \frac{Q_{ss} Q_{\psi\psi} - Q_{s\psi}^2}{s^2} + \frac{2Q_\psi Q_{s\psi}}{s^3} - \frac{Q_\psi^2}{s^4} \quad (8)$$

This is the polar form of H (Ref. 25). Appendix A has a derivation of (8). The caustic surface is generated by the contour of W that satisfies $H \rightarrow 0$ in (8). The expression for the caustic surface is (6) evaluated for the contour of W , where $H = 0$. In the far zone ($z \rightarrow \infty$), $Q \approx -W$, and H becomes the Gaussian curvature of W in the paraxial approximation.^{21,25}

B. Review of the formation and properties of axisymmetric toroidal wave fronts

Backscattering from spheres can be predominately due to radiation from a wave front of the form shown in Fig. 1(a) (Refs. 1–11). This scattering is often referred to as glory scattering^{1,8,12,14} because the circular interference fringes produced by the wave front form a “glorifying” halo.

The expression for the toroidal wave front shape [Fig. 1(a)] is

$$\tilde{W}(s) = -[\Lambda + (s - b)^2/2\alpha], \quad (9)$$

where Λ is a constant [in Fig. 1(a), $\Lambda < 0$], α is the radius of curvature of \tilde{W} in the s direction for $s \approx b$, and the significance of the parameter b is noted below. This expression is two-term Taylor series expansion for a general smooth toroidal wave front shape. Backpropagating the wave front a distance α shows that the wave front appears to emanate from a ring source of radius b [Fig. 3(a)]. The amplitude of a periodic wave field resulting from this wave front is proportional to (Ref. 2) $J_0[kb \sin \gamma z / (\alpha + z)]$, as seen also by the first term of (28) and (29) below with the perturbation parameter $\delta = 0$. Radiation from \tilde{W} is axially focused on the z axis. That is, some annular contour of \tilde{W} having a radius $s \leq b$ is focused to some point on the z axis. Hence, the caustic surface associated with \tilde{W} is referred to as an axial caustic.^{11,12} An infinite number of rays from this contour came to focus.^{11,12} The zero Gaussian-curvature contour generates upon propagation, the far zone or directional caustic.²¹ This is the contour indicated by the ring at $s \approx b$ in Fig. 1(a). On this contour, \tilde{W} is locally flat in the azimuthal direction for $s \approx b$, hence, rays emanating from this contour spread negligibly on propagation to the far zone. Away from the axis, two rays labeled 1 and 2 contribute in a given direction. These geometrical properties of \tilde{W} can be readily verified by using the expression for \tilde{W} in Eqs. (6) and (8).

The wave front \tilde{W} occurs in the backward and forward scattering of sound by fluid and elastic spheres.^{1–6} It also is

C. Formation and applications of two-fold symmetric harmonically perturbed toroidal wave fronts

Our present study of properties of harmonically perturbed toroidal wave fronts was motivated by observations of backscattering by freely rising oblate spheroidal bubbles in water.¹⁴ In those observations, bubble oblateness was a controllable factor within a certain range of bubble sizes. Larger bubbles rose faster than smaller bubbles and, hence, took on a more oblate shape. From physical arguments (reviewed below), the perturbed toroidal wave front shape pertinent in the light backscattering by slightly oblate bubbles is well approximated by

$$W(s, \psi) = \bar{W}(s) - f_1(\psi), \quad (10a)$$

$$f_1(\psi) = (\delta/2)(1 + \cos 2\psi), \quad (10b)$$

where $\bar{W}(s)$ is given by (9). The perturbation parameter δ is the difference in height between points where the rays 1 and 4 contact W in Fig. 1(b). Generally, δ need not be positive. Figure 3(b) is the virtual source shape that the wave front of Fig. 1(b) appears to emanate from.

The expression for W given in (10) is the wave front shape appropriate for light or sound reflecting from a distorted torus of the type shown in Fig. 3(b) when the incident wave is directed along the $-z$ axis. The torus has two-fold symmetry about the z axis.

The perturbation function $f_1(\psi)$ is related to the first term in a perturbation series devised by Berry [Eq. (37) of Ref. 21] to unfold the axial caustic associated with $\bar{W}(s)$. In our notation, Berry's conjectured first term is $f_1 = \epsilon_0 s^2 \cos(2\psi)$, where ϵ_0 is a constant. The s^2 factor in his f_1 term is not present in the unfolding considered here.

Backscattering of waves by a slightly oblate object will be used in the remainder of Sec. I C to illustrate how W of (10) can be produced. Figure 5 is a model of glory ray paths^{1,10,11,14} in a penetrable oblate spheroid with refractive index $\mu < 1$. The interior of the object may either be a homogeneous fluid¹ or solid.^{2,3} In the latter case, the internal rays may represent directions of either longitudinal or shear waves. Figure 5(a) shows the elliptical profile of the scatterer seen from the z axis. Here, $R(\psi, z=0)$ is the radius of the elliptical profile in the plane at $z=0$. Distances a and d are the semimajor and semiminor axis lengths. Figure 5(b) is the cross section of the spheroid lying in the y', z' plane. The path of a glory ray in this profile is sketched. Figure 5(c) is the cross section of the spheroid lying in the x', z' plane. An oblateness factor defined as

$$\Gamma_0 = a^2/d^2 - 1 \quad (11)$$

characterizes spheroids shapes, which are oblate for $d < a$ and prolate for $d > a$.

A plane through the spheroid tilted by the angle ψ also intersects the surface to give an ellipse. The local oblateness of this ellipse is $\Gamma(\psi) = a^2/R(\psi, 0)^2 - 1$, where $\Gamma(0) = \Gamma_0$ and $\Gamma(\pi/2) = 0$. It can be demonstrated that

$$\Gamma(\psi) = \Gamma_0(1 + \cos 2\psi)/2 \quad (12)$$

exactly, and, hence, that

$$R(\psi, 0) = a/[1 + \Gamma(\psi)]^{1/2} \approx a[1 - \Gamma(\psi)/2] + O(\Gamma_0^2). \quad (13)$$

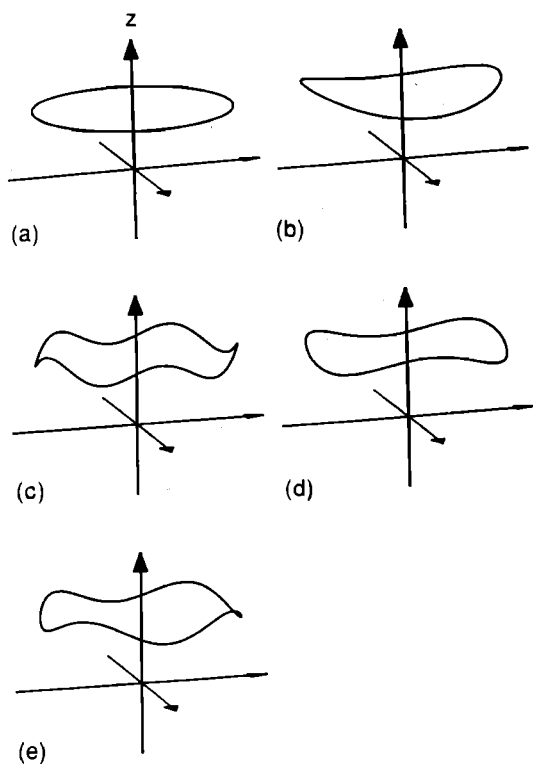


FIG. 3. The wave front of Eq. (15) appears to emanate from virtual sources with shapes shown in (a)–(e) for $p = 0, 2, 4, 3$, and 5 , respectively. (a)–(d) are the virtual source locations that wave fronts (a)–(d) in Fig. 1 appear to emanate from. (a) is the axisymmetric virtual source location of the unperturbed wave front given by Eq. (9). Reflected light or sound from torii with core shapes shown in (b)–(e) should give caustics shown in Fig. 7(a), (b), (d), and (e), respectively, in an observation plane (Fig. 2) with constant z .

pertinent to light scattering by spherical drops or bubbles in the same scattering directions.^{7–11} A toroidal wave front shape can also occur when sound is reflected from a torus.^{26,27} The reflecting axicon^{15–19} shown in Fig. 4 and discussed in Appendix B can also give a toroidal wave front.

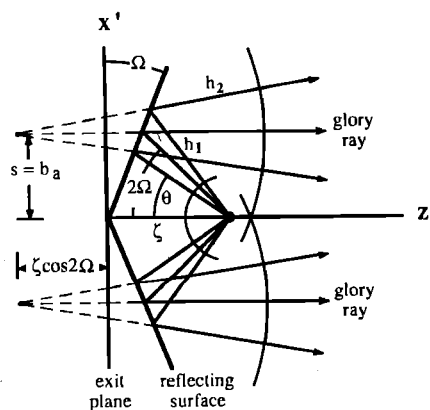


FIG. 4. Geometry of the reflecting axicon. A point source is located a distance ζ from the apex of a reflecting cone. By inspection, the reflected wave front appears to emanate from a focal circle (rotate this figure about the z axis) of radius b . The outgoing wave front is given by (B3) for $s \approx b$, and is shown in Fig. 1(a). The wave front shape becomes that of Fig. 1(b) if the point source is slightly off of the z axis or if the cone generating angle Ω is the function of the azimuthal angle ψ discussed in the Appendix B.

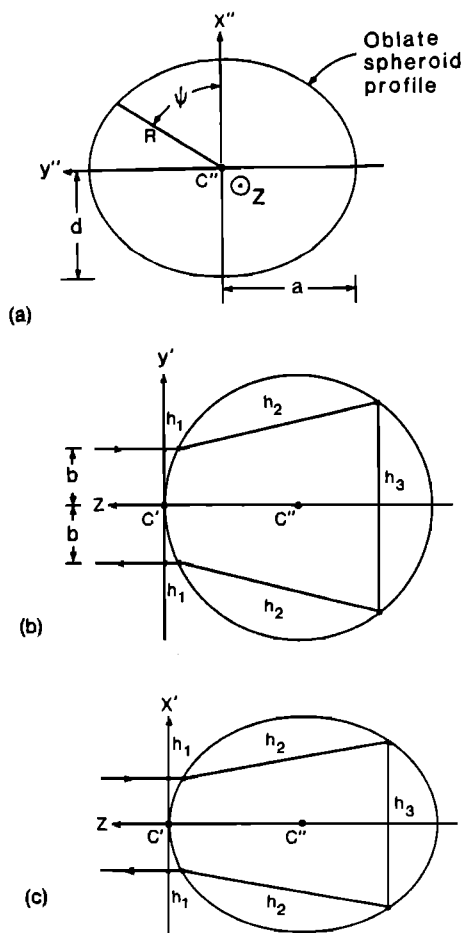


FIG. 5. Model for the production of transmitted glory rays in two planes of a penetrable oblate spheroidal scatterer for which the internal sound speed exceeds that of the surroundings. The (x'', y'', z) system has its origin at the centroid of the oblate object, point C'' . The (x', y', z) system's origin is point C' . (a) Elliptical profile of the oblate spheroid in the plane containing the axis x'' of rotational symmetry. The profile $R(\psi, z=0)$ is given in Eq. (13). (b) Path of a glory ray in the circular cross section of the oblate spheroid that contains the y' and z axis. The location of C' and C'' are shown to aid comparison of these cross-sectional views. (c) Path of a glory ray in the elliptical cross-section of the oblate spheroid that contains the x' and z axis. Glory rays of the type shown in (b) and (c) only exist in these two planes of the oblate spheroid when the incident wave travels in the $-z$ direction.

Equations (11)–(13) characterize geometric features of the scatterer.

Let the outgoing wave front from a sphere of radius a be the unperturbed case given by (9). Now flatten the sphere to give a slightly oblate spheroid. An argument for the use of an approximate perturbation function of the form $f_1(\psi)$ in (10) will now be given. Rays that leave parallel to the axes, as shown in Fig. 5(b) and (c), occur only in these two planes of the oblate spheroid. These *glory rays* are confined to a single plane, their respective planes of incidence. Rays incident in planes at $\psi \neq 0$ or $\pi/2$ are not confined to a single plane and are called *skew rays*. Denote the *difference* in the propagation phase delay of glory rays in the x', z and y', z planes as $k\delta$. As shown in Fig. 5, δ is given by

$$\delta = [2h_1 + \mu(2h_2 + h_3)]_{\text{ellipse}} - [2h_1 + \mu(2h_2 + h_3)]_{\text{circle}}, \quad (14)$$

where the first and second terms refer to distances h_j defined in Fig. 5(c) and (b), respectively. Except in the circular plane $\psi = \pi/2$, the wave front is advanced as a result of the flattening. Along the glory ray in the $\psi = 0$ plane, it is advanced a distance $-\delta$. For $\Gamma_0 \ll 1$, numerical ray tracing discussed below supports the limited use of an approximation in which any dependence of the wave front perturbation on s is neglected. This gives W as in (10a) in which the focal parameters b and α used in the evaluation of (9) are taken to be independent of ψ . Numerical results computed from the usual rules of ray tracing show that δ is linear in Γ_0 , where δ is related to Γ_0 through (14) and $\Gamma_0 \ll 1$. From the aforementioned advancement of the wave front for $\psi = 0$, it follows that $f_1(\psi)$ should also be linear in $\Gamma(\psi)$. Inspection of (12) shows that (10b) meets these requirements.

The approximate nature of (10) is evident by considering the impact parameters for the glory rays shown in Fig. 5(b) and (c). Since the cross section is circular in Fig. 5(b), the impact parameter has the unperturbed value b . For the elliptical profile in Fig. 5(c), it has the value b_e (not shown on the figure). Numerical ray tracing for $\mu = 0.75$ shows that $(b_e - b)/b$ is linear in Γ_0 when $\Gamma_0 \ll 1$. Furthermore, for the purpose of approximating the near-backward directed parts of W , it can be satisfactory to neglect the difference of b_e and b , as well as any ψ dependence of α . We obtained agreement among experimental observations and computations on applying these approximations to backscattering of light by oblate bubbles¹⁴ for which $\Gamma_0 \lesssim 0.01$. While these approximations may not be very robust, they are sufficient to motivate the form of (10). Even if we were to take b and α as weakly dependent on ψ , the topology of the farfield caustics should not be affected for $\Gamma_0 \ll 1$.

The considerations above should also apply to slightly prolate spheroids as well. In Appendix B, we describe how wave fronts in the form of (10) arise from perturbations of the axicon of Fig. 4.

D. Generalization of Sec. C to p -fold symmetric wave fronts

The oblate spheroid, reflecting torus, and distorted reflecting cone mentioned above are twofold symmetric objects about their z axis. We can generalize the present study to include wave fronts that are p -fold symmetric about their z axis, with $p = 2, 3, \dots$. The $p = 4$ and 3 wave fronts are shown in Fig. 1(c) and (d). The general form of the harmonically perturbed wave front is taken to be

$$W(s, \psi) = \bar{W}(s) - f(\psi), \quad (15a)$$

$$f(\psi) = (\delta/2)(1 + \cos p\psi), \quad (15b)$$

where δ may be positive or negative and $\bar{W}(s)$ is given by (9). The $p = 2$ wave front is $W(s, \psi)$ in (10). The part of f that unfolds the axial caustic $(\delta/2)\cos(p\psi)$. For definiteness, we restrict our attention to perturbations described by the f of (15). Our choice for the form of f was made so that when $p = 1$, $f = f_1$ of (10b). In Sec. I E, we show that taking $p = 1$ only shifts the direction of the farfield caustic.

An alternate way of harmonically perturbing W is to take b in (9) to be $b(\psi) = b_0(1 + \epsilon \cos p\psi)$, where b_0 is constant and $\epsilon \ll 1$. We do not consider this class of perturba-

tion because its use leads to terms of order ϵ^2 in the perturbation of $\tilde{W}(s \approx b_0)$ and it is less germane to problems of interest. We anticipate, however, that it leads to caustics having features similar to those described here.

Reflections from distorted torii, as shown in Fig. 3 for $p = 2 - 5$, have wave fronts given by (15). The cross-sectional diameter of the torus^{26,27} determines α in (9). The amount of distortion permissible for the present theory to be applicable can be computed from the inequality in (21). In constructing a wave front of the form (15) for the back-scattering by a distorted torus, we assume the exit plane is near the distorted torus and use a paraxial approximation as in Ref. 27. The reflected wave is described by a phase shift of the incident wave just as in the standard treatment of thin lenses in Ref. 20. A distorted torus centered around $(x', y', z) = [b \cos \psi, b \sin \psi, f(\psi/2)]$ should give a wave front of the form (15) for $\delta \ll b$.

When p is even, (15) is applicable to scattering from a three-dimensional (3-D) penetrable object whose boundary is given by

$$R(\psi, z) = (a^2 - z^2)^{1/2} / [1 + (\Gamma_0/2)(1 + \cos p\psi)]^{1/2} \\ \approx (a^2 - z^2)^{1/2} [1 - (\Gamma_0/4)(1 + \cos p\psi)], \quad (16)$$

where Γ_0 , given by (11), is taken to be small relative to unity. Note that $R(\psi, z)$ vanishes for $z = \pm a$. The distances a and d in (11) are the maximum and minimum values of $R(\psi, 0)$, respectively; that is, $a = R(\psi = \pi/p, 0)$ and $d = R(\psi = 0, 0)$. Profiles of the object in the plane $z = 0$ correspond to curves $R(\psi, 0)$ and are shown in Fig. 6. When $p = 2, 4, 6, \dots$, the object has p -fold symmetry about the z axis, and inversion symmetry about the origin. These symmetry properties can be confirmed by inspection of Fig. 6(a)–(c), which are for $p = 2, 4$, and 6 . The mirror symmetry planes pass through the objects cross sections as shown and are parallel to the z axis. It is the inversion symmetry (i.e., center of symmetry¹³), combined with the other symmetries mentioned above, that allows us to extend and generalize the arguments given in Sec. I C and Fig. 5 to objects with $p > 2$ and p even. Glory rays of the same type as those shown in Fig. 5 occur in each of the mirror symmetry planes in Figs. 6(a)–(c) because the objects' surface normals all lie in these planes. For even p , the intersection of the object and a mirror symmetry plane is in ellipse for angles $\psi = 0, 2\pi/p, 4\pi/p, \dots$, and the intersection is a circle for angles $\psi = \pi/p, 3\pi/p, 5\pi/p, \dots$. The objects defined by (16) when $p > 2$ cannot be generated by rotation of the section shown in Fig. 6 about the z axis.

Figure 6(d) and (e) are the cross sections of the $p = 3$ and $p = 5$ objects generated by (16). These objects, and the others for p odd, do not have the inversion symmetry of the even p objects. The restriction to even p occurs because the odd p objects generated by (16) do not have cross sections of circles or ellipses in the mirror symmetry planes. Thus the generalization of the glory ray concepts in Sec. I C are not applicable to odd p objects.

The argument given in Sec. I C for the formation of a wave front given by (10) and shown in Fig. 1(b) for a slightly spheroidal scatterer can be extended and generalized as

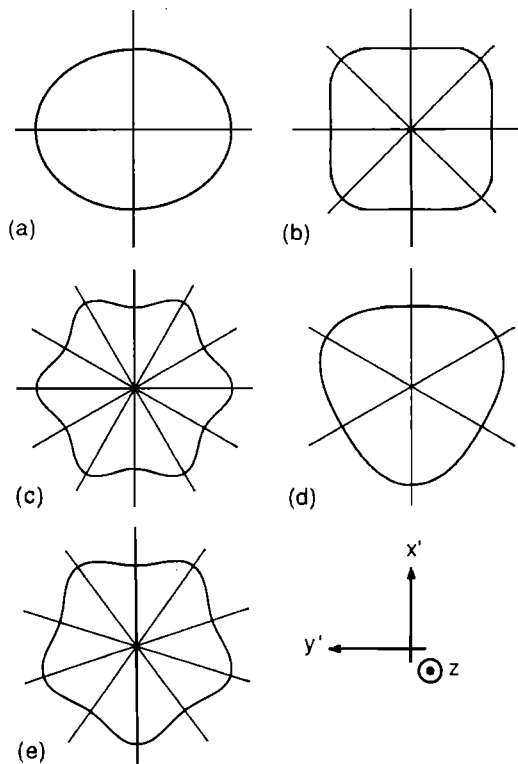


FIG. 6. Object profiles $R(\psi, z = 0)$, described by Eq. (16) with $p = 2, 4, 6, 3$, and 5 for (a)–(e), respectively. The objects have p -fold rotational symmetry about the z axis, and mirror symmetry about p planes containing the z axis and the lines shown. The even p objects have an additional inversion symmetry about the centroid of the object. The cross sections of even p objects in the mirror symmetry planes are circles and ellipses. This allows a generalization of the glory rays concepts of Fig. 5 when p is even. The cross sections of odd p objects in their mirror symmetry planes are half-ellipses connected smoothly to half-circles. Hence, the glory rays will not be the same as those shown in Fig. 5.

follows to objects with boundaries given by (16) with p even. Consider a spherical scatterer that is known to produce the axisymmetric toroidal wave front shown in Fig. 1(a). Each circular cross section of the sphere can produce glory rays as shown, for example, in Fig. 5(b). Deform the sphere to a boundary given by (16) with p even. The intersections of the deformed object and the mirror symmetry planes [Fig. 6(a)–(c)] are circles and ellipses that produce glory rays. For sufficiently small deformations, the wave front should have a form commensurate with the object's geometrical shape. Such wave fronts are given by (15). The perturbation parameter δ has the same interpretation as given in (14) above.

In Sec. I E we will not be concerned with other mechanisms for producing $W(s, \psi)$, but will concentrate on its propagation properties. The primary result of this article is to obtain the caustic surface of $W(s, \psi)$ given by (15) and the associated wave fields.

E. Caustic surface of the harmonically perturbed toroidal wave front

The caustic surface can be calculated by determining the contour of W , which satisfies $H \rightarrow 0$ in (8), for given z , and using this contour in the ray equation (6). To simplify the

calculation, note that, for W given by (15), Q in (7) can be written

$$Q(s, \psi, z) = \Lambda + \frac{\delta}{2} + \frac{b^2}{2(\alpha + z)} + \frac{[s - b(\bar{\alpha}/\alpha)]^2}{2\bar{\alpha}} + \frac{\delta}{2} \cos p\psi, \quad (17)$$

where $\bar{\alpha}(z)$ is the reduced quantity

$$\bar{\alpha} = \alpha z / (\alpha + z). \quad (18)$$

The contour $s = b\bar{\alpha}/\alpha$ is the contour of the unperturbed wave front $\tilde{W}(s)$ given by (9) which comes to focus a distance z from the reference plane. Then, use of (17) in (8) gives an expression

$$q^4 - \frac{\bar{\alpha}}{\alpha} q^3 - \frac{\bar{\alpha}}{\alpha} \beta p^2 q^2 \cos p\psi - \left(\frac{\bar{\alpha}}{\alpha} p\beta \sin p\psi \right)^2 = 0 \quad (19)$$

for the $H \rightarrow 0$ condition, where $q(\psi) = s/b$ locates rays to the caustic and

$$\beta = \delta\alpha/2b^2. \quad (20)$$

It is trivial to numerically solve (19) for $q(\psi)$ and an exact analytical solution is algebraically messy and unenlightening. An approximate solution can be obtained when the inequality

$$|\beta| p^2 (\alpha/\bar{\alpha}) \lesssim 0.025 \quad (21)$$

is valid. This solution is

$$q(H=0) \approx \bar{\alpha}/\alpha + p^2\beta \cos p\psi + O(\beta^2) \quad (22)$$

Then, using (22) in the ray equation (6), the caustic surface is given parametrically by

$$U = (p\beta b/2\bar{\alpha}) \{ (p-1) \cos[(p+1)\psi] + (p+1) \cos[(p-1)\psi] \}, \quad (23a)$$

$$V = (p\beta b/2\bar{\alpha}) \{ (p-1) \sin[(p+1)\psi] - (p+1) \sin[(p-1)\psi] \}. \quad (23b)$$

In a given observation plane, with z constant, the figure produced by Eqs. (23) has $2p$ cusps for p even and p cusps for p odd. Several of these caustics are shown in Fig. 7. The $p=2$ solution appropriate for the oblate scatterers discussed above in Sec. I C is given by

$$U^{2/3} + V^{2/3} = [(2\delta/b)(\alpha/\bar{\alpha})]^{2/3}. \quad (24)$$

For fixed z , (24) is an equation for a four-cusped curve known as an astroid. This caustic is shown in Fig. 7(a). The z dependence of (24) occurs through (18). The inequality expressed in (21) gives the acceptable geometry for which the approximate form (23) is valid. Larger values of p give a wave front with more curvature, hence, it is reasonable that (21) depends on p as shown. Equations (21) and (24) were verified for $p=2$ by numerically solving the exact forms (19) and (6) for the caustic surface.

When $p=1$, Eq. (23) is still applicable. In this case, however, the perturbation does not unfold the axial caustic. The wave front given by (15) with $p=1$ is a tilted version of the axisymmetric wave front in Fig. 1(a). Accordingly, use of (23) gives an axial caustic with tilt given by $x = zU = \delta(\alpha+z)(2b)^{-1}$ and $y = zV = 0$. Hence, $p=2$

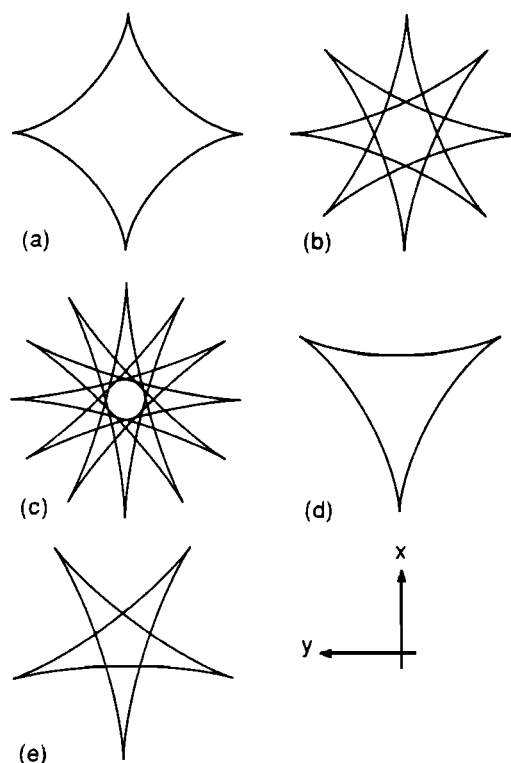


FIG. 7. Caustics for wave front perturbations having $p = 2, 4, 6, 3,$ and 5 in (a)–(e), respectively, for a plane with $z = \text{constant}$. The caustics were computed from Eq. (23). The even p caustics in this plane have p -fold rotational and mirror symmetry and inversion symmetry about their centers. The odd p caustics lack the inversion symmetry. The odd p caustics are degenerate: They are traced out twice when ψ ranges from 0 to 2π in (23). Hence, while even p wave fronts have $2p$ outer cusps, odd p wave fronts have only p outer cusps.

has the simplest symmetry for a perturbation that unfolds the caustic.

For $p > 2$ and even, in a plane of constant z , the caustic is a $2p$ pointed star as shown in Fig. 7(b) for $p=4$. For $p=3$, the caustic in a plane with z constant is a hypocycloid with three cusps [Fig. 7(d)]. The $p > 3$, with p odd, caustics in this plane are stars with p cusps. This collection of “celestial” caustics beautifully unfold the structurally unstable²¹ axial caustic associated with the wave front shown in Fig. 1(a).

II. WAVE FIELD, CALCULATED RESULTS, AND INVERSE SCATTERING

A. Fresnel approximation for the wave field

Rayleigh–Sommerfeld diffraction theory in the Fresnel approximation²⁰ can be used to understand the propagation properties of the wave field associated with the wave front given by (15). The validity condition is that the observation plane must be at z such that z such that $z^3 \gg kb^4/2\pi$ and, loosely, that the observation angle γ is not too large. The analysis shown here is similar to that done by Fujiwara¹⁷ for the image of an off-axis point source produced by the reflecting axicon shown in Fig. 4. See also Ref. 2, where the authors performed a similar nearfield calculation for the wave front given by (9). Denote the pressure by P . The appropriate

diffraction integral is^{1,2,11,20}

$$P(\gamma, \varphi) = P_0 \frac{k}{2\pi i} \frac{\exp[ik(r + \Lambda + \delta/2)]}{r} \times \int_0^\infty \exp\left(\frac{iks^2}{2z}\right) s ds \int_0^{2\pi} \exp[-ikW(s, \psi)] \times \exp[-iks \sin \gamma \cos(\varphi - \psi)] d\psi, \quad (25)$$

where P_0 is the amplitude at the exit plane and the time factor $\exp(-i\omega t)$ has been suppressed. This is a polar form of the diffraction integral where $\tan \gamma \approx \sin \gamma$ has been used, and $W(s, \psi)$ is given by (15). Use of (17) in (25) gives the form

$$P(\gamma, \varphi) = P_0 \frac{k}{2\pi i} \frac{\exp(ikr)}{r} \int_0^\infty s ds \int_0^{2\pi} \exp[ikQ(s, \psi)] \times \exp[-iks \sin \gamma \cos(\varphi - \psi)] d\psi. \quad (26)$$

The angular integral is

$$B(s; \gamma, \varphi) = \frac{1}{2\pi} \int_0^{2\pi} \exp[-iks \sin \gamma \times \cos(\psi - \varphi)] \exp\left(i \frac{k\delta}{2} \cos p\psi\right) d\psi. \quad (27)$$

Neumann's factor used below is defined as $\epsilon_0 = 1$, $\epsilon_{n \neq 0} = 2$. Use of the Jacobi expansion²⁸

$$\exp\left(i \frac{k\delta}{2} \cos p\psi\right) = \sum_{n=0}^{\infty} \epsilon_n i^n J_n\left(\frac{k\delta}{2}\right) \cos(np\psi),$$

and the integral result²⁸

$$\int_0^{2\pi} \exp[-iks \sin \gamma \cos(\psi - \varphi)] \cos np\psi d\psi = 2\pi(i)^{np} J_{np}(ks \sin \gamma) \cos(np\varphi),$$

gives the expression

$$B(s; \gamma, \varphi) = \sum_{n=0}^{\infty} \epsilon_n i^{n(p+1)} J_n\left(\frac{k\delta}{2}\right) J_{np}(ks \sin \gamma) \cos(np\varphi). \quad (28)$$

When $\delta = 0$, $B(s; \gamma, \varphi) = J_0(ks \sin \gamma)$, which is the correct form for the unperturbed toroidal wave front.¹ When $p = 1$, an addition theorem for Bessel functions²⁸ gives $B(s; \gamma, \varphi) = J_0[u^2 + (k\delta/2)^2 + k\delta u \cos \varphi]^{1/2}$ for (28) where $u = ks \sin \gamma$. This expression arises because the axial caustic is only tilted when $p = 1$ [see the discussion below Eq. (24)].

The radial integral can be approximated using the method of stationary discussed in Appendix B of Ref. 1. A typical integral for the n th term of the series (28) is approximated as

$$\int_0^\infty \exp\left(ik \frac{[s - b(\bar{\alpha}/\alpha)]^2}{2\bar{\alpha}}\right) J_{np}(ks \sin \gamma) s ds \approx b \frac{\bar{\alpha}}{\alpha} \left(\frac{2\pi i \bar{\alpha}}{k}\right)^{1/2} J_{np}\left(kb \frac{\bar{\alpha}}{\alpha} \sin \gamma\right) \exp\left(i \frac{k\bar{\alpha} \sin^2 \gamma}{2}\right)$$

by use of the stationary phase approximation. The resulting

expression for the pressure is

$$P(\gamma, \varphi) \approx P_0 \frac{\exp[ik(r + \Lambda + \delta/2)]}{r} \times \exp\left(i \frac{kb^2}{2(\alpha + z)}\right) \exp\left(-i \frac{k\bar{\alpha} \sin^2 \gamma}{2}\right) \times b \frac{\bar{\alpha}}{\alpha} \left(\frac{2\pi i \bar{\alpha}}{k}\right)^{1/2} B\left(b \frac{\bar{\alpha}}{\alpha}; \gamma, \varphi\right), \quad (29)$$

where B is given as in (28) but for the indicated argument. This expression is valid for the same inequality expressed in (21); this limit to the validity of (29) exists because the stationary phase approximation was used. Convergence of the series in (28) is assured by the $J_n(k\delta/2)$ factor. For $n \gg k|\delta|/2$, the series in (28) is (absolutely) rapidly monotonically decreasing for increasing n .

B. Caustic properties and computed angular scattering patterns

The caustics for $p = 2, 4, 6, 3$, and 5 are shown in Fig. 7(a)–(e). The caustics correspond to virtual sources such as those shown in Fig. 3, and scattering from the objects with even p profiles shown in Fig. 6. They were calculated for an observation plane at a fixed distance z from an exit plane (see Fig. 2). The even p caustics have $2p$ cusps, and the odd caustics have p cusps.

When p is odd, U and V in (23) are invariant under the transformation $\psi \rightarrow \psi + \pi$. Thus odd p caustics can be generated by varying ψ from 0 to π from π to 2π . The caustics associated with the odd p wave fronts [for example Fig. 1(d)] given by (15) are degenerate and are thus unstable with respect to slight deformations of the wave front. The wave front for $p = 3$ is shown in Fig. 1(c). The wave fronts for $p = 3$ and 5 appear to emanate from virtual sources with shapes shown in Fig. 3(d) and (e).

The wave field of (29) has been computed for the $p = 2$ term in Figs. 8 and 9 for several representative values of kb and δ/b . The observation plane was taken to be in the far zone in these calculations. When $p = 2$ the wave front is Fig. 1(b). Figure 8(a) was computed for $kb = 30$, $\alpha/b = 0.075$, and $\delta b = -0.1$. The minus sign has no special significance here, but implies an oblate, rather than prolate, scatterer for the specific case of backscattering of light by bubbles.¹⁴ In Fig. 8(b), the astroid caustic, generated by (24) has been overlaid on the wave field. The wavelength used in this calculation is approximately a third of the maximum wave length that just resolves effects of the perturbation in the wave field [see the discussion below (31)]. Hence, the effects of the perturbation are relatively mild in comparison with Fig. 9(b) and (c).

Figure 9(a)–(c) are wave field and caustic calculations for $\delta/b = -0.02$, $\alpha/b = 0.025$, and $kb = 100, 500$, and 1000 , respectively. The wavelength used in Fig. 9(a) just barely shows any effects of the perturbation in the angular scattering pattern. The wavelength used in Fig. 9(c) was a tenth of that used in Fig. 9(a). In this figure, the amplitude of fringes nearest the caustic, especially near the cusps, is greater than other regions. The caustic clearly separates regions of the diffraction pattern for which different numbers

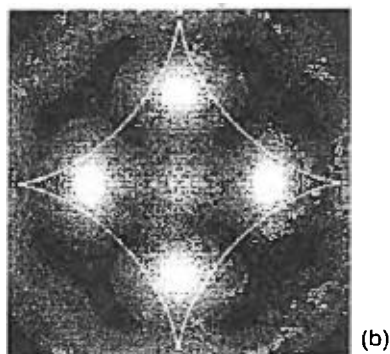
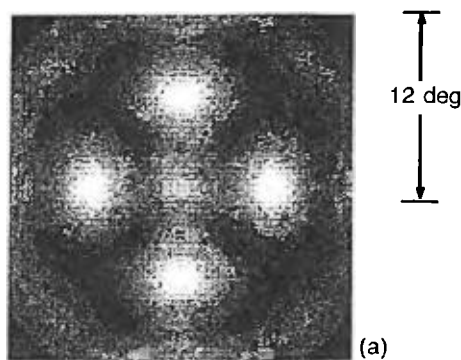


FIG. 8. (a). Angular wave field pattern of $|P(\gamma, \varphi)|^2$ computed from Eq. (29) with $p = 2$ for $kb = 30$, $\alpha/b = 0.075$, $\delta/b = -0.1$, and z in the far zone. The image was produced using 200×200 pixels each having 1 of 10 gray scales that range linearly in $|P|^2$ from white, for the largest value, to black, for the smallest value. (b) The astroid caustic of Eq. (24) has been overlaid on the wave field calculation of (a) showing how the caustic is manifested in the wave field for relatively small values of kb . By comparison, for unperturbed wave fields, P is simply proportional to $J_0(kx \sin \gamma)$ and does not depend on φ .

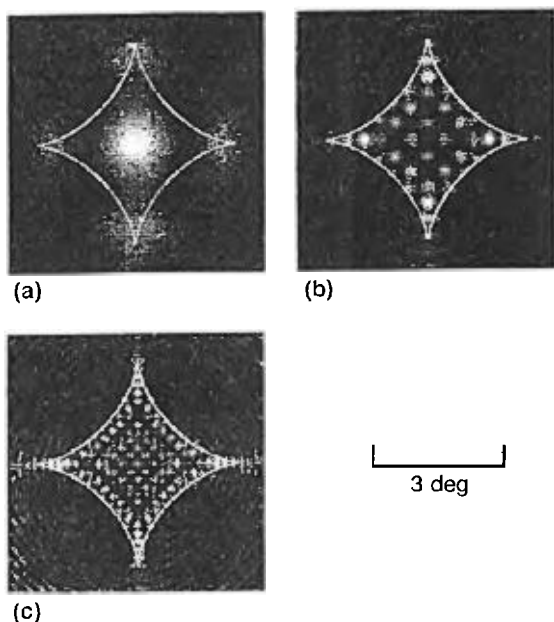


FIG. 9. Wave field and caustics patterns, calculated in the same way as Fig. 8, for parameters $\alpha/b = 0.25$, $\delta/b = -0.02$, and (a) $kb = 100$, (b) $kb = 500$, and (c) $kb = 1000$. The caustic is better resolved in the wave field for increasingly larger values of kb .

of rays interfere: On the inside of the caustic, four-rays interfere, and two rays interfere on the outside of the caustic as discussed in Sec. III.

C. Inverse problems and a localization principle

A condition on the wavelength necessary to just resolve observable effects of the perturbation parameter δ can be obtained from (29) and (23). When $\delta = 0$, the first zero of the angular scattering pattern occurs for

$$kb(\bar{\alpha}/\alpha)\sin \gamma \approx 2.405. \quad (30)$$

Now from (23), a cusp point is located at

$$U = \tan \gamma \approx \sin \gamma = (|\delta|/2b)(\alpha/\bar{\alpha})p^2. \quad (31)$$

Using (31) in (30), the wavelength must satisfy $\lambda \lesssim |\delta|p^2$ for a cusp point to be beyond the first zero of the J_0 Bessel function, and, hence, small enough to just resolve effects of δ in the angular scattering pattern. *Equivalently, significant distortion of the pattern requires that $|\delta| \gtrsim \lambda/p^2$.*

A "localization" principle⁷ can be applied to the series in (28) to estimate the spacing of fringes in the azimuthal direction for fringes near the caustic (see Fig. 10). From the properties of Bessel functions, the main contribution to the series should occur for $n = k|\delta|/2$. From the cosine term in this series, the azimuthal fringes are spaced by angles $n\pi\Delta\varphi = \pi$ when $\Delta\varphi$ is small. Eliminating n between these expressions gives

$$\Delta\varphi = 2\pi p k b |\delta/b|. \quad (32)$$

This expression matches physical intuition: When δ/b or $kb \rightarrow 0$, there are no azimuthal fringes, and small wavelengths or large perturbations (kb and $|\delta/b| \gg 1$ respectively) give many fringes. This expression is tested below. Different scatterers with the same product $kb\delta/b$ have the same characteristic fringe spacing azimuthally; However, the radial fringe spacing has an additional $(kb)^{-1}$ dependence.

At a cusp point, it is reasonable to expect, by the same localization principle, that both $n = k|\delta|/2$ and $n\pi = kb \sin \gamma \bar{\alpha}/\alpha$ should be true simultaneously so that both of the Bessel functions in (28) have their orders equal to their

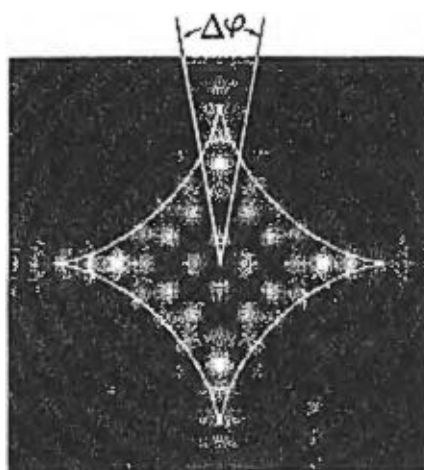


FIG. 10. The wave field pattern was calculated for the same parameters as in Fig. 9(b). The definition of the angular displacement $\Delta\varphi$ is shown.

arguments. Eliminating n between these expressions reproduces the cusps angle given in (31) (from the geometrical solution), which bolsters the use of the localization principle.

The localization principle used to obtain (32) can be tested in Fig. 10. Consider the bright fringe near the upper most cusp point in this figure. The angular width of this fringe (i.e., the angle subtended by the first null on the left to the first null on the right of this bright fringe, as measured from the center of the pattern) is predicted to be $\Delta\varphi = 18$ deg from use of (32). Measurement of the fringe width on the figure gives $\Delta\varphi = 19 \pm 2$ deg. The uncertainty in this measurement arise because the exact location of the fringe nulls are not well defined.

Assuming that the cusp angle and azimuthal fringe spacing near the cusp of one of the outer caustics in (23) are known from experimental data, $|\delta/b|$ and kb can be inferred from (31) and (32). From (31) it follows that $|\delta/b| = 2 \sin \gamma_{\text{cusp}}/p^2$ and from this and (32) that $kb = p\pi/(\Delta\varphi \sin \gamma_{\text{cusp}})$ where $z \gg \alpha$, thus $\bar{\alpha}/\alpha \approx 1$, has been assumed for ease of expression. These expressions for $|\delta/b|$ and kb give the geometric characteristics of the scatterer from observables in the angular scattering patterns. For these expressions to be useful, the wavelength must be small enough to give sufficiently detailed angular scattering patterns [i.e., the discussion below (31)].

Determination of δ from wave field data can be used to infer the oblateness Γ_0 . We have demonstrated this in the analogous problem of light scattering from oblate bubbles in water.¹⁴ For scattering of sound from penetrable objects with shapes for which p is even in (16), δ/b should be linear in the oblateness factor Γ_0 of (11) as $\delta/b = D\Gamma_0$. Here, D is dependent upon the specific scattering mechanism, be it a surface wave, or bulk transmitted wave, which allows the formation of glory rays in the mirror symmetry planes of the objects shown in cross section in Fig. 6. Here, D can be computed theoretically from an analysis such as (14) for bulk transmitted waves,^{1,2,3} or from GTD⁶ for surface waves.

III. LOCATIONS OF RAYS CONTRIBUTING NEAR THE CUSP POINTS FOR THE ASTROID CAUSTIC

Rays are defined by (2). They are normal to \mathcal{W} and pass through the observation point (x,y,z) . There may be several or no rays that pass through a given observation point. In this section, the types of rays (skew or planar) contributing to the pressure amplitude at several specific observation points will be defined and discussed. Here, \mathcal{W} refers to the wave front given by (10) or by (15) with $p = 2$. The section of the caustic surface shown in Fig. 11(a) is the farzone caustic of \mathcal{W} . When the observation point is located in the far zone, ($z \gg kb^2/2$) the Hessian of (8) reduces to the Gaussian curvature of \mathcal{W} .²¹ Thus it is the projection of rays from the zero Gaussian-curvature contour of \mathcal{W} , which generates the far zone caustic.²¹ The purpose of Fig. 11 is to show how rays merge as the observation point approaches and passes over the caustic surface. Appendix C contains the equations describing these curves. These idealized rays can be observed in analogous optical experiments by viewing the exit plane from a point in the observation plane.²⁹ In acoustics, rays

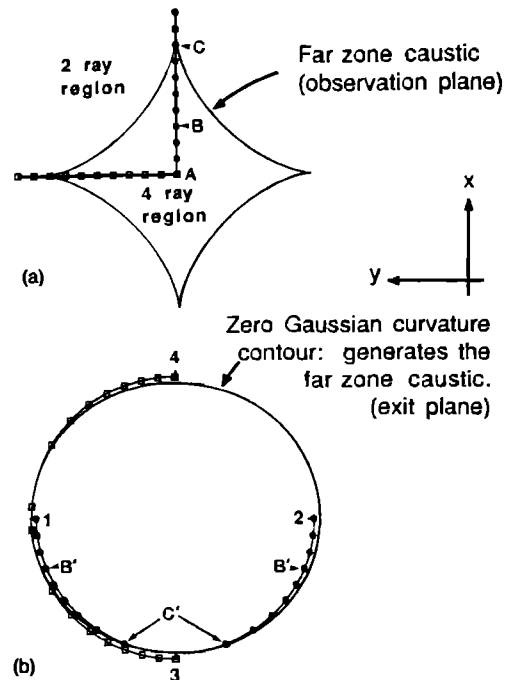


FIG. 11. (a) Directional or far-zone caustic generated by the zero Gaussian-curvature contour (ZGCC) for the wave front of Fig. 1(b). By looking toward the exit plane in the $-z$ direction, from observation points arising from the origin of this figure, and moving in the x or y direction, the rays that contribute to the scattering in a given direction can be identified. (b) The slightly elliptical curve is the projection of the ZGCC of Fig. 1(b) onto the exit plane. The other contours represent rays that point to the observation plane as discussed in Sec. IV. Ray trajectories were computed as described in Appendix C.

near and on caustics can be identified by using time-resolved pulses of sound.^{29,30}

Figure 11(a) illustrates the far zone caustic and two paths along the observation plane that cross the caustic at the cusp points. Figure 11(b) is a projection onto the exit plane of several contours of \mathcal{W} . The slightly elliptical contour in Fig. 11(b) is the zero Gaussian-curvature contour (ZGCC) of \mathcal{W} computed from (22). This contour is sketched on the wave front in Fig. 1(b). Rays projected normally from \mathcal{W} along this contour generate the far zone or directional caustic shown in Fig. 11(a). The half-ellipse contour, which has circle markers on it, starts at 1 and 2 and moves closer to the ZGCC. Rays from points 1 and 2 on this contour pass through point A of the caustic figure in Fig. 11(a). Consider the consequence of moving the observation point in the positive x direction up to point B, taking unit steps marked by the circles. The skew rays (i.e., rays that do not lie in the x,z plane, the plane which contains the observation point under consideration), which pass through a given point along this path, come from the half-ellipse contour at intervals marked by the circles. The skew rays to B come from the points marked B'. The cusp lies just beyond point C. As the observation point nears C, the skew rays from this contour move to C'. Beyond C' the skew rays merge with the ZGCC and become focused at the cusp point. When the observation point passes beyond the cusp point into the two-ray region, the skew rays no longer exist. This merging of

rays is similar to that discussed for an isolated cusp in Ref. 23.

There are also two planar rays (i.e., rays which have trajectories lying wholly in the x,z plane) that pass through the observation points marked by circles. Planar rays originate on W above the short line segments in the x,z plane. These segments are shown in Fig. 11(b) and start at the center of the squares labeled 3 and 4. As the observation point moves from A–C and beyond into the two-ray region, the planar rays pass through these observation points. Since these rays are spaced far apart, their interference gives finely spaced fringes.

Consider now the path in the observation plane which starts at A and is marked by squares lying along the y axis. This path has 2 skew rays that start at the center of the squares at 3 and 4. It has two planar rays that start the center of the circles at 1 and 2. The skew rays merge with the ZGCC as the observation point approaches the cusp point as described above. When the observation point passes over the cusp point and into the two-ray region, only the planar rays remain. Note that the skew ray contour and the observation plane path both lie in the *same* half-space ($y > 0$) for this case and in *opposite* half-spaces for the contour and path considered above.

IV. DISCUSSION AND CONCLUSION

Caustics are catastrophic in the sense that^{21,22} the gradient map defined by (2) is singular on the surface $H \rightarrow 0$, where H is given by (3). In wave propagation, the caustic surface separates regions of space where different numbers of rays contribute to the scattering.^{21,22} Hence, the nature of the diffraction pattern changes “catastrophically” on passage across the caustic surface. Figure 9(c) illustrates this point succinctly, where the caustic surface separates a four-ray region on the interior of the caustic and a two-ray region on the exterior of the caustic. The astroid and star caustics shown in Fig. 7 are not elementary catastrophes as described in Ref. 21–24, 30, and 31. Catastrophe theory is, however, useful for classifying features of these caustics as noted below.

In Ref. 23, Marston discussed the general form of a wave front that propagates to produce a transverse cusp diffraction catastrophe. To make a connection between Ref. 23 and this article, consider the local region of W given by (10) near $\psi = 0$; that is, the local region of W surrounding the point where ray 4 in Fig. 1(b) contacts W , including the small section of the zero Gaussian-curvature contour also. This region has the same general shape as the wave front shown in Fig. 4 of Ref. 23 and is given by Eq. (9) in Ref. 23. To verify this, W of (10) is expanded in Cartesian coordinates about the point ($s = x' = b, \psi = 0$). Using Cartesian coordinates defined by $(\xi, \eta) = (x' - b, y')$ the local region of W under consideration is given by $W(\xi, \eta) = -\xi^2/2\alpha - \delta(1 - \eta^2 + 2\xi\eta^2)$. Comparing this expression with the generic expression given in Eq. (9) of Ref. 23, we find that $W(\xi, \eta)$ has a form that gives a transverse cusp. This region of W propagates to produce a portion of the astroid caustic in the vicinity of the cusp located at the azimuthal angle $\varphi = \pi$ (as

discussed in Sec. III). Periodic wave fronts having the generic form described in Ref. 23 propagate to produce wave fields described by the Pearcey function. In the present work, the wave field is clearly similar to form to the Pearcey function [compare Fig. 9(c) with, e.g., Fig. 13 of Ref. 31 or Fig. VII of Ref. 32]. Differences are attributable to the existence of an extra background ray in the present work. The Pearcey function describes the wave field of three rays interfering on one side of the cusp caustic, and 1 ray on the other. In the present work, the caustic separates regions of four-ray and two-ray interference as shown in Fig. 11(a).

The comments above also apply to the local regions of W near rays 1–3 in Fig. 1(b). Taken separately, these regions of W and their associated caustics belong to the cusp class of elementary catastrophes.^{21–23} Each hump and depression of the wave fronts shown in Figs. 1(c) and 1(d), for which $p = 4$ and 3, also produces cusps for a total of eight and six cusps, respectively. For the $p = 3$ wave front, however, cusps produced by parts of the wave front at say, $\psi = \psi_0$ and $\psi = \psi_0 + \pi$, lie on top of one another in the observation plane. Hence, of the six cusps produced by the wave front in Fig. 1(d), only 3 are visible, as shown in Fig. 7(d), because of this overlapping of caustics.

In Sec. 6 of Ref. 21, Berry uses the axisymmetric wave front given by (9) as an example of a wave front whose caustic is of infinite codimension. An infinite number of topologically different ways to unfold the axisymmetric wave front of (9) implies an infinite codimension²¹ for the axial caustic associated with (9). Specific examples are the distinct p in (15). The elementary catastrophes of catastrophe optics do not describe caustics of infinite codimension.²¹ The wave fronts of Fig. 1 and the caustics of Fig. 7 are not described *globally* by any of the classes of elementary diffraction catastrophes. (However, as shown above, we may use catastrophe optics for *local* regions of W .) Thus the caustic shown in Fig. 7(d) cannot be a section of the elliptic umbilic catastrophe.^{21,31} To further this point, note that a localized slight tilting of the wave front in Fig. 1(d) will break its three-cusped caustic into a further series of cusped caustics, the number dependent on the perturbation. However, a slight perturbation of wave fronts that propagate to produce elliptic umbilic catastrophes^{21,31} does not further unfold an elliptic umbilic into a multicusped figure. The fact that both the elliptic-umbilic caustic and the $p = 3$ caustic have the same form is apparently only an interesting coincidence. Berry’s comment in Sec. 6 of Ref. 21, “...then the point caustic should break up into closed cusped figures, the number of cusps depending on the topology of ...,” has been demonstrated in Fig. 7(a)–(e) and (23).

We used an oblate spheroid with sound speed *greater* than its surrounding as an example in Fig. 5. Consider now a spherical scatterer with sound speed *less* than that of the surrounding media. Let $\mu > 1$ be the ratio of sound speed in the surrounding media to the sound speed in the scatterer. For $(2)^{1/2} < \mu < 2$, it can be shown that a circular cross section of the sphere can produce glory rays having two chords^{1,32} [compare to the three-chord glory ray model, where $\mu < 1$, for the circular cross section in Fig. 5(b)]. Thus, for μ in this range, a sphere can produce a backward

directed wave front that is locally similar to the toroidal wave front in Fig. 1(a). Then, the wave front shape for a slightly oblate scatterer for which $(2)^{1/2} < \mu < 2$ will be that of Fig. 1(b). Thus our analysis for its unfolded caustic applies to this problem as well. The fact that the unfolded glory for this case becomes an astroid was anticipated for this specific example in Nye's catastrophe theoretic analysis.³³

Chaudhuri *et al.*,³⁴ used ray tracing to study glory rays (i.e., exactly backward directed rays) for the analogous problem of electromagnetic backscattering by dielectric spheroids having $\mu \approx 1.78$. They found that when the object shape changes from spherical to spheroidal, the number of glory rays changes from essentially infinite to a small number. The number of glory rays for spheroids depends on its orientation relative to the incident beam. They conclude³⁴: "Also, on the basis of the numerical analysis it appears reasonable to contend that in the studies involving backscattering from nonspherical dielectric objects, one needs almost never be concerned with the glory ray component." It is true that there are few exactly backward directed rays, in general, for spheroidal scatterers. However, we wish to emphasize that the axial caustic does not just disappear for spheroidal scatterers. The axial caustic unfolds to the astroid caustic shown in Fig. 7(a). *Significant focusing can occur even for nonspherical scatterers.*

An asymmetric astroid caustic [analogous to a stretched version of Fig. 7(a)] can be observed in the scattering of light³⁵ or sound³⁶ by an opaque (or rigid in the case of sound) elliptical disk. The *boundary of the ellipse* is a (real) source of edge diffracted rays.³² For plane-wave incidence, the caustic surface of the edge diffracted rays is a *cylindrical surface* whose cross section is the evolute of the ellipse,³⁵⁻³⁸ which is an astroid. This is not an example of the problem analyzed in Secs. I-III since the (virtual) source associated with the wave front in Fig. 1(b) is the *two-fold symmetric bent ring* shown in Fig. 3(b). According to (24), the caustic surface of this wave front has an astroid cross section in which the cusp points *move away from* the axis as z increases. For general $p > 2$, the cusp points described by (24) also move away from the axis with increasing z . Cylindrical caustic surfaces with cross sections as shown in Fig. 7 should, however, result when light or sound is scattered by disks with boundaries shown in Fig. 6. This should occur because the evolute of $R(\psi, 0)$ appears to be proportional to (23) for sufficiently small Γ_0 . Hence, the aforementioned edge diffraction caustics should be generalizable to the $p > 2$ caustics of Fig. 7.

Some other examples of astroid caustics are noteworthy though the mechanisms for producing them differ in detail from the ones considered in this article. Sections of a huge astroid caustic were observed in the occultation of the star ϵ Geminorum by the planet Mars.³⁹ The observations were made by use of a telescope in an airborne observatory, which was in Mars' shadow. The Martian atmosphere acts as a lens with appreciable spherical aberration.⁴⁰ In general, spherical aberration unfolds the perfect point focus of an ideal lens into a line caustic.^{22,40} The oblateness of Mars causes an astigmatism that further unfolds the line caustic into a surface with an astroid cross section.^{40,41} This experiment can

also be performed using an Earth source of radio waves; the occultation can be measured behind planets (or stars in principle) with space probes.⁴¹ Occultation data can be used to infer physical properties (such as temperature and pressure profiles) of planetary atmospheres.^{39,41}

In conclusion, we have considered the detailed propagation properties of harmonically perturbed toroidal wave fronts shown in Figs. 1(b)-(d) and given by (15). The caustic surfaces associated with these wave fronts were computed in Sec. I and the wave fields in Sec. II. Applications to inverse scattering were also given in Sec. II. Ray properties of the wave front were discussed in Sec. III. The catastrophe optics of the perturbed wave fronts and their associated caustics were considered in Sec. IV. This work is relevant to scattering by slightly oblate or prolate spheroids and other p -fold symmetric scatterers given by (16) when p is even, to reflections from distorted torii, to axicons (like Fig. 4), and to other scatterers that have p -fold symmetry about an axis.

ACKNOWLEDGMENT

This research was supported by the Office of Naval Research.

APPENDIX A: CONVERSION OF THE HESSIAN TO POLAR COORDINATES

The Hessian in Cartesian coordinates is given by (3). For ϕ most naturally expressed in polar coordinates, such as (5) in the present work, it is useful to have the polar form of H . The conversion of H from Cartesian coordinates to polar coordinates is facilitated by the following relations:

$$\begin{aligned} x' &= s \cos \psi, & y' &= s \sin \psi, \\ s^2 &= x'^2 + y'^2, & \psi &= \tan^{-1}(y'/x'). \end{aligned}$$

The first partials are

$$\phi_{x'} = \frac{\partial s}{\partial x'} \phi_s + \frac{\partial \psi}{\partial x'} \phi_\psi = \cos \psi \phi_s - \left(\frac{\sin \psi}{s} \right) \phi_\psi,$$

and

$$\phi_{y'} = \frac{\partial s}{\partial y'} \phi_s + \frac{\partial \psi}{\partial y'} \phi_\psi = \sin \psi \phi_s + \left(\frac{\cos \psi}{s} \right) \phi_\psi.$$

The partials needed to form the Hessian in polar coordinates are

$$\begin{aligned} \phi_{x'x'} &= \cos^2 \psi \phi_{ss} + \frac{\sin 2\psi}{s^2} \phi_{\psi\psi} \\ &\quad - \frac{\sin 2\psi}{s} \phi_{s\psi} + \frac{\sin^2 \psi}{s} \phi_{ss} + \frac{\sin^2 \psi}{s^2} \phi_{\psi\psi}, \end{aligned} \quad (\text{A1})$$

$$\begin{aligned} \phi_{y'y'} &= \sin^2 \psi \phi_{ss} - \frac{\sin 2\psi}{s^2} \phi_{\psi\psi} \\ &\quad + \frac{\sin 2\psi}{s} \phi_{s\psi} + \frac{\cos^2 \psi}{s} \phi_{ss} + \frac{\cos^2 \psi}{s^2} \phi_{\psi\psi}, \end{aligned} \quad (\text{A2})$$

and

$$\begin{aligned} \phi_{x'y'} &= \frac{\sin 2\psi}{2} \phi_{ss} - \frac{\cos 2\psi}{s^2} \phi_{\psi\psi} \\ &\quad + \frac{\cos 2\psi}{s} \phi_{s\psi} - \frac{\sin 2\psi}{2s} \phi_{ss} - \frac{\sin 2\psi}{2s^2} \phi_{\psi\psi}. \end{aligned} \quad (\text{A3})$$

Straightforward use of (A1)–(A3) in (3) gives the polar form

$$H = \frac{\phi_s \phi_{ss}}{s} + \frac{\phi_{ss} \phi_{\psi\psi} - \phi_\psi^2}{s^2} + \frac{2\phi_\psi \phi_{s\psi} - \phi_\psi^2}{s^3}. \quad (\text{A4})$$

This expression is rotationally invariant, as it must be, by inspection, because an angular transformation of the form $\psi \rightarrow \psi + \psi_0$, where ψ_0 is a constant angle, does not change the form of (A4). Equation (A4) reduces to Eq. (8) when ϕ is paraxially approximated by (4).

The validity of using the paraxial approximation for the purpose of locating caustics was recently examined by Dangelmayr and Wright.⁴² Since the cusps predicted here are generally transverse to the outgoing wave fronts, their analysis suggests that our use of the paraxial approximation, Eq. (4), is valid.

APPENDIX B: WAVE FRONTS PRODUCED BY REFLECTING AXICONS

Axicon imaging systems^{15–19} of the type shown in Fig. 4 produce axial caustics. A point source is located a distance ζ from the vertex of the reflecting cone. The outgoing toroidal wave front appears to emanate from a ringlike source. In this Appendix, we give a novel analysis of the wave front parameters in Eq. (9) and describe how harmonic perturbations can arise. Though our analysis is new, certain results may be implicit in previous discussions. We include this Appendix to show how Eqs. (9) and (15) can give insight into a variety of problems.

The direction of reflected rays in Fig. 4 follows from the usual condition that the angle of incidence and reflection are equal. The launch angle of a ray from the source is θ . When $\theta = 2\Omega$, it may be shown that the ray is reflected parallel to the z axis at a radius $b = \zeta \sin 2\Omega$ from the axis. Such rays are referred to as glory rays in analogy with scattering problems. Let $h_1(s_c, z_c)$ denote the distance from the point source to an arbitrary point on the cone having radial and z coordinates of (s_c, z_c) denote the distance along the reflected ray to a specific wave front of interest. The requirement that the wave front be an equiphase surface gives

$$h_1(s_c, z_c) + h_2(s, W) = h_c, \quad (\text{B1})$$

where h_c is a constant. It is convenient to take $h_c = 2\zeta$. Then, glory rays have $h_1 = h_2 = \zeta$. We are interested in the wave front formed by the rays launched at $\theta \approx 2\Omega$. A geometrical construction yields the following parametric solution of (B1),

$$W(\theta) = 2\zeta \cos(\theta - 2\Omega) + z_v, \quad (\text{B2a})$$

$$s(\theta) = 2\zeta \sin(\theta - 2\Omega) + b, \quad (\text{B2b})$$

where $z_v = -\zeta \cos 2\Omega$. Combining (B2a) and (B2b), the wave front is given by

$$W(s) = z_v + 2\zeta \left[1 - \left(\frac{s-b}{2\zeta} \right)^2 \right]^{1/2} \\ \approx 2\zeta + z_v - \frac{1}{2} \frac{(s-b)^2}{2\zeta}. \quad (\text{B3})$$

Inspection of (B3) shows that the wave appears to diverge

from a ringlike source at $z = z_v$. Equation (B3) is the equation of a circle of radius 2ζ centered at the virtual image of the point source (see Fig. 4) as expected. This is the same general form W given in (9). This wave front shape is common to most of the other axicon imaging systems discussed by McLeod.¹⁵

An axicon can produce a wave front given by (10) and shown in Fig. 1(b) in two ways. When the point source in Fig. 4 is moved slightly off of the z axis, the resulting wave front near the exist plane is given by (10) (Ref. 17). This shape should also occur when the cone angle Ω in Fig 4 depends on the azimuthal angle. Let $\Omega(\psi) = \Omega_0 + A f_1(\psi)$, where Ω_0 is a constant angle, $f_1(\psi)$ is given in (10b), and A is a constant such that $|A\delta| \ll 1$. Use of $\Omega(\psi)$ in the z_v term of (B3) gives W as in (10a), where δ describes the amplitude of the wave front perturbation and $A = (2\zeta \sin 2\Omega_0)^{-1} \equiv (2b_0)^{-1}$. Since $b_0 = \zeta \sin 2\Omega$, the term $(s-b)^2/4\zeta$ also depends on ψ . This dependence is of order δ^2 and may be neglected when δ is small. The form of $\Omega(\psi)$ considered here can be thought of as an astigmatism type of aberration of the axicon imaging system.

Rayces¹⁶ reasoned that the image produced by an axicon imaging system of a point source off of the optical axis is the astroid caustic of (24). By geometric construction, McLeod (1960)¹⁵ showed that a two-fold symmetric axicon, such as the one discussed above, produces an astroid image of an on axis point source.

APPENDIX C: SKEW AND PLANAR RAY CONTOURS ON THE INITIAL WAVE FRONT

In this Appendix, we show how the skew ray, planar ray, and zero Gaussian-curvature contour in Fig. 11(b) were computed. When the observation plane is in the far zone, the distance function (5) can be approximated as $\phi(s, \psi; \gamma, \varphi) = r - W(s, \psi) - s \sin \gamma \cos(\psi - \varphi)$. The extremum condition (2) can be written as $\phi_s = 0$ and $\phi_\psi = 0$ in polar coordinates. Use of W from Eq. (10) in these extremum conditions gives

$$s = b + \alpha \sin \gamma \cos(\psi - \varphi), \quad (\text{C1a})$$

$$\delta \sin 2\psi = s \sin \gamma \sin(\psi - \varphi), \quad (\text{C1b})$$

respectively. Equations (C1a) and (C1b) are coupled equations for contours of the initial wave front W , given by (s, ψ) , which emanate rays that pass in the observation direction (γ, φ) . Observation direction coordinates γ and φ are chosen as independent variables. Equations (C1) locate rays (there may be up to four such rays) having the direction (γ, φ) of interest.

Planar rays, by definition, satisfy $\psi = \varphi$ and $\psi = \pi + \varphi$ so that they lie in a single plane. Use of these conditions in (C1a) and (C1b) gives

$$s = b \pm \alpha \sin \gamma, \quad (\text{C2a})$$

$$\sin 2\psi = 0, \quad (\text{C2b})$$

where the plus sign refers to $\psi = \varphi$. Equation (C2b) can be satisfied for $\psi = 0$ and π for the observation plane path lying on the x axis in Fig. 11(a) (i.e., $\varphi = 0$ or π), or for $\psi = \pi/2$ and $3\pi/2$ for the path lying on the y axis (i.e., $\varphi = \pi/2$ or

$3\pi/2$). The planar rays paths are given by (C2a) for these values of ψ .

In Fig. 11(b), we have chosen to investigate the skew rays contributing along the observation plane path with circles as markers. These rays are given by (C1a) and (C1b) when $\varphi = 0$. They are classified as skew rays because we have relaxed the planarity condition that $\psi = 0$ or π . These expressions can be solved simultaneously to give

$$s = \frac{2\delta b}{2\delta - \alpha \sin^2 \gamma}, \quad \cos \psi = \frac{b \sin \gamma}{2\delta - \alpha \sin^2 \gamma}, \quad (\text{C3})$$

for $\varphi = 0$, and

$$s = \frac{2\delta b}{2\delta + \alpha \sin^2 \gamma}, \quad \sin \psi = \frac{-b \sin \gamma}{2\delta + \alpha \sin^2 \gamma}, \quad (\text{C4})$$

for $\varphi = \pi/2$ (the observation plane path marked with squares). The skew and planar ray paths in Fig. 11 were computed from use of (C2)–(C4). When $\delta = 0$, there are no skew rays, which is the expected result for a spherical (or more general, axisymmetric) scatterer.

- ¹P. L. Marston and D. S. Langley, "Glory- and rainbow-enhanced acoustic backscattering from fluid spheres: Models for diffracted axial focusing," *J. Acoust. Soc. Am.* **73**, 1464–1475 (1983); **78**, 1128 (1985).
- ²P. L. Marston, K. L. Williams, and T. J. B. Hanson, "Observation of the acoustic glory: High-frequency backscattering from an elastic sphere," *J. Acoust. Soc. Am.* **74**, 605–618 (1983).
- ³K. L. Williams and P. L. Marston, "Mixed-mode acoustical glory scattering from a large elastic sphere: Model and experimental verification," *J. Acoust. Soc. Am.* **76**, 1555–1563 (1984).
- ⁴K. L. Williams and P. L. Marston, "Axially focused (glory) scattering due to surface waves generated on spheres: Model and experimental confirmation using tungsten carbide spheres," *J. Acoust. Soc. Am.* **78**, 722–728 (1985).
- ⁵K. L. Williams and P. L. Marston, "Backscattering from an elastic sphere: Sommerfeld–Watson transformation and experimental confirmation," *J. Acoust. Soc. Am.* **78**, 1093–1102 (1985); "Synthesis of backscattering from an elastic sphere using the Sommerfeld–Watson transformation and giving a Fabry–Perot analysis of resonances," *J. Acoust. Soc. Am.* **79**, 1702–1708 (1986).
- ⁶P. L. Marston, "GTD for backscattering from elastic spheres and cylinders in water and the coupling of surface elastic waves with the acoustic field," *J. Acoust. Soc. Am.* **83**, 25–37 (1988).
- ⁷H. C. Van de Hulst, "A theory of the anti-corona," *J. Opt. Soc. Am.* **37**, 16–22 (1947); *Light Scattering by Small Particles* (Wiley, New York, 1957).
- ⁸V. Khare and H. M. Nussenzveig, "Theory of the glory," *Phys. Rev. Lett.* **38**, 1279–1282 (1977); H. M. Nussenzveig, "Complex angular momentum theory for the rainbow and the glory," *J. Opt. Soc. Am.* **69**, 1068–1079 (1979).
- ⁹D. S. Langley and P. L. Marston, "Glory in optical backscattering from air bubbles," *Phys. Rev. Lett.* **47**, 913–916 (1981).
- ¹⁰P. L. Marston and D. S. Langley, "Forward optical glory from bubbles (and clouds of bubbles) in liquids and other novel directional caustics," in *Multiple Scattering of Waves in Random Media and Random Rough Surfaces*, edited by V. V. Varadan and V. K. Varadan (Pennsylvania State U. P. University Park, PA, 1987), pp. 419–429.
- ¹¹W. P. Arnott and P. L. Marston, "Optical glory of small freely-rising gas bubbles in water: Observed and computed cross-polarized backscattering patterns," *J. Opt. Soc. Am. A* **5**, 496–506 (1988).
- ¹²M. V. Berry, "Uniform approximations for glory scattering and diffraction peaks," *J. Phys. B* **2**, 381–392 (1969).
- ¹³For a discussion of the symmetry terminology used here, see, e.g., J. F. Nye, *Physical properties of crystals* (Oxford U. P., Oxford, 1985), Appendix B.
- ¹⁴W. P. Arnott and P. L. Marston, "Backscattering of laser light from freely rising spherical and spheroidal air bubbles in water, in *Ocean Optics IX*, edited by M. A. Blizard, *Proc. Soc. Photo-Opt. Instrum. Eng.* **925**, 296–307 (1988). (It is our intent to give a more detailed description of the experiments in a manuscript in preparation. These experiments support the generalization of the present article's results to the more complicated problem of cross-polarized backscattering by oblate bubbles.)
- ¹⁵J. H. McLeod, "The axicon: A new type of optical element," *J. Opt. Soc. Am.* **44**, 592–597 (1954); "Axicons and their uses," *J. Opt. Soc. Am.* **50**, 166–169 (1960).
- ¹⁶J. L. Rayces, "Formation of axicon images," *J. Opt. Soc. Am.* **48**, 576–578 (1958).
- ¹⁷S. Fujiwara, "Optical properties of conic surfaces. I. Reflecting cone," *J. Opt. Soc. Am.* **52**, 287–292 (1962).
- ¹⁸J. W. Y. Lit and E. Brannen, "Optical properties of a reflecting cone," *J. Opt. Soc. Am.* **60**, 370–371 (1970).
- ¹⁹C. B. Burckhardt, H. Hoffman, and P. -A. Grandchamp, "Ultrasound axicon: A device for focusing over a large depth," *J. Acoust. Soc. Am.* **54**, 1628–1630 (1973).
- ²⁰J. W. Goodman, *Introduction to Fourier-Optics* (McGraw-Hill, New York, 1968).
- ²¹M. V. Berry, "Waves and Thom's Theorem," *Adv. Phys.* **25**, 1–26 (1976).
- ²²M. V. Berry and C. Upstill, "Catastrophe optics: Morphologies of caustics and their diffraction patterns," in *Progress in Optics*, edited by E. Wolf (North-Holland, Amsterdam, 1980), Vol. 18, 257–346.
- ²³P. L. Marston, "Transverse cusp diffraction catastrophes: Some pertinent wave fronts and a Pearcey approximation to the wave field," *J. Acoust. Soc. Am.* **81**, 226–232 (1987); **83**, 1976 (1988).
- ²⁴P. L. Marston, "Cusp diffraction catastrophe from spheroids: Generalized rainbows and inverse scattering," *Opt. Lett.* **10**, 588–590 (1985).
- ²⁵C. E. Dean, W. P. Arnott, and P. L. Marston, "Principal curvatures of general wavefronts and of reflecting or refracting surfaces," *J. Acoust. Soc. Am. Suppl. 1* **83**, S59 (1988). The explicit expressions are given in this abstract. (These expressions should be useful for computing curvatures of wave fronts most naturally expressed in polar coordinates.)
- ²⁶J. B. Keller and D. S. Ahluwalia, "Diffraction by a curved wire," *SIAM J. Appl. Math.* **20**, 390–405 (1971).
- ²⁷P. L. Marston, "Half-order derivative of a sine-wave burst: Applications to two-dimensional radiation, photoacoustics, and focused scattering from spheres and a torus," *J. Acoust. Soc. Am.* **76**, 291–295 (1984).
- ²⁸G. N. Watson, *Theory of Bessel Functions* (Cambridge U. P., New York, 1944).
- ²⁹P. L. Marston, "Surface shapes giving transverse cusp diffraction catastrophes in acoustic or seismic echoes," in *Acoustical Imaging Vol. 16*, edited by L. W. Kessler (Plenum, New York, 1988), pp. 579–588.
- ³⁰M. B. Brown, "The transient wave fields in the vicinity of the cuspid caustics," *J. Acoust. Soc. Am.* **79**, 1367–1384 (1986).
- ³¹M. V. Berry, J. F. Nye, and F. J. Wright, "The elliptic umbilic diffraction catastrophe," *Philos. Trans. R. Soc. London Ser. A* **291**, 453–484 (1979).
- ³²S. Solimeno, B. Crosignani, and P. DiPorto, *Guiding, Diffraction, and Confinement of Optical Radiation* (Academic, Orlando, FL, 1986).
- ³³J. F. Nye, "Rainbow scattering from spheroidal drops—An explanation of the hyperbolic umbilic foci," *Nature (London)* **312**, 531–532 (1984).
- ³⁴S. K. Chaudhuri, F. B. Sliator, and W. M. Boerner, "Analysis of internally reflected and diffracted fields in electromagnetic backscattering by dielectric spheroids," *Radio Sci.* **19**, 987–999 (1984).
- ³⁵J. Coulson and G. G. Becknell, "Reciprocal diffraction relations between circular and elliptical plates," *Phys. Rev.* **20**, 594–600 (1922); "An extension of the principle of the diffraction evolute, and some of its structural detail," *Phys. Rev.* **20**, 607–612 (1922).
- ³⁶R. Dong, L. Adler, and P. A. Doyle, "Observations of diffraction caustics for ultrasound," *J. Appl. Phys.* **54**, 2832–2834 (1983).
- ³⁷P. A. Doyle, "Diffraction by discs for a point source in the near field," *Opt. Acta* **30**, 323–346 (1983).
- ³⁸See Ref. 32, Fig. V.24.
- ³⁹J. L. Elliot, R. G. French, E. Dunham, P. J. Gierasch, J. Veverka, C. Church, and C. Sagan, "Occultation of ϵ Geminorum by Mars. II. The structure and extinction of the Martian upper atmosphere," *Astron. J.* **217**, 61–679 (1977).
- ⁴⁰M. V. Berry, "Singularities in waves and rays," in *Physics of Defects*, edited by R. Balian, M. Kleman, and J. P. Poirier (North-Holland, Amsterdam, 1981), pp. 453–543. See pp. 485 and 499.
- ⁴¹V. R. Eshleman, G. L. Tyler, and W. T. Freeman, "Deep radio occultations and evolute flashes; their characteristics and utility for planetary studies," *Icarus* **37**, 612–626 (1979).
- ⁴²G. Dangelmayr and F. J. Wright, "On the validity of the paraxial eikonal in catastrophe optics," *J. Phys. A* **17**, 99–108 (1984).